Proceedings IRF2018: 6th International Conference Integrity-Reliability-Failure
Lisbon/Portugal 22-26 July 2018. Editors J.F. Silva Gomes and S.A. Meguid
Publ. INEGI/FEUP (2018); ISBN: 978-989-20-8313-1

PAPER REF: 7118

STRAIN-RATE INFLUENCE ON A SHAPE MEMORY ALLOY BASED DAMPER

João Morais(*), Carlos Santos, Paulo Morais
Scientific Instrumentation Centre, National Laboratory for Civil Engineering (LNEC), Lisboa, Portugal
(*)*Email:* jmorais@lnec.pt

ABSTRACT

This paper describes the dynamic tests performed on an energy dissipation damper based on Shape Memory Alloy (SMA) wires. It continues the mechanical characterization process of this device started in a previous study (Morais, 2017). The aim of the study described in this paper is to evaluate the strain-rate and temperature influence on the device's damping capability, as groundwork for a more complete test in a shaking table. The underlying concept of this device is the use of a double counteracting system of pre-strained SMA wires as the dissipation elements. By using pre-strained wires, this design is focused on maximizing energy dissipation, partially relinquishing the re-centring capabilities of the device. The experimental tests were performed on a downscaled prototype, already used in the aforementioned study.

In parallel with these tests, a constitutive model was developed for this device, based on the SMA mechanical and kinetic laws described in the literature (Lobo, 2015), in order to complement future design projects based on this damper configuration.

Keywords: vibration damper, shape memory alloy, earthquake response.

INTRODUCTION

Passive energy dissipation techniques have shown to be an effective strategy when aimed at structural preservation against seismic events. These systems are designed to eliminate or at least to reduce structural damage on buildings and infrastructures by absorbing part of the energy of the seismic event. One energy dissipation technique consists on using dampers based on SMA wires. Shape Memory Alloys have several interesting properties that can be exploited in these applications, namely their superelasticity, high fatigue resistance and near strain-rate independence, depending on a suitable temperature control (Dolce, 2000).

Superelasticity is the main property explored in this type of devices and represents the capability of the material to transform between metallurgical phases (austenitic and martensitic phases) due to external stress application. The forward transformation corresponds to the change from austenite to martensite, as opposed to the inverse transformation that corresponds to the change from martensite to austenite. This property allows SMA based dampers to withstand very large strains (when compared to dampers based on other metallic materials) without any residual deformation upon unloading, while dissipating energy during the loading/unloading cycles.

According to the available literature, SMA based dampers can be affected by temperature and strain-rate variations (Dolce, 2000). Namely, if the temperature or the strain-rate increases,

the damper can exhibit a reduction on its damping capabilities. This study aims to evaluate how these parameters affect the damping capability of our device.

DAMPER'S CONCEPT DESCRIPTION

The passive energy dissipation damper developed for this project uses two bundles of SMA wires in a double counteracting arrangement, with pre-strain applied to both wire bundles. We chose this type of configuration because it focuses on maximizing the energy dissipation while maintaining the external load (measurable load exerted by the damper when actuated) on predictable levels (Dolce, 2001). These preliminary tests were performed on a downscaled prototype of the original design (Figure 1) with Nitinol austenite SMA wires (Ø1.75 mm). This device is described in full detail in our previous article regarding this subject (Morais, 2017).

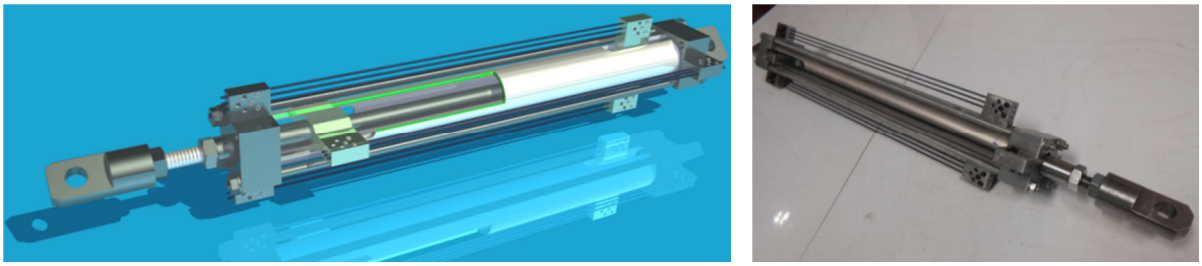

Fig. 1 - (left) virtual representation of the fully assembled prototype and (right) a photograph of the manufactured device

CONSTITUTIVE MODEL FOR THE DAMPER

Over the years, several researchers have dedicated their time to create accurate constitutive models to describe the behaviour of SMA wires (see some examples in Lobo, 2015). These models can vary in complexity and applicability, but ultimately they should allow the user to predict the complex SMA behaviour, if the proper material parameters are used.

SMA constitutive models feature one mechanical law, one kinetic law, and one thermal balance equation in the case of rate-dependant models. The mechanical law relates stress (σ), strain (ε), temperature (T) and martensite fraction (ξ), as a function of the material's Young Module (E) and thermal expansion coefficient (θ). Martensite fraction is an internal state variable that represents the extent of the forward transformation in the SMA, i.e. the percentage of SMA that has been transformed into martensite (M) from austenite (A). The kinetic law mathematically describes the evolution of the martensite fraction as a function of stress and temperature changes, based on the material's stress-temperature phase diagram. The thermal balance equation describes the temperature changes in the SMA, taking into account the heat exchanges with the surrounding environment and the heat generated by the SMA during the loading cycles.

In an attempt to consolidate our knowledge on this device, a preliminary rate-dependent constitutive model was developed based on the models by Auricchio and Tanaka (Auricchio, 2006 and Tanaka, 1986). The mechanical law (Equation 1) created using the Voight formulation describes the behaviour of the device, more specifically, the resulting external stress and the interactions between the two wire bundles (subscript *1* and *2*). This model uses a linear kinetic law (Equation 2 and 3) to determine the martensitic fraction of the SMA wires

during the metallurgical phase transformations. Equation 4 represents the thermal balance equation used in this constitutive model.

$$\Delta\sigma = [\xi_1 E_M + (1-\xi_1)E_A](\varepsilon_1 - \varepsilon_L\xi_1) - [\xi_2 E_M + (1-\xi_2)E_A](\varepsilon_2 - \varepsilon_L\xi_2) + \theta(T_1 - T_2) \quad (1)$$

$$\text{Austenite to Martensite: } \xi = \frac{|\sigma| - \sigma_s^M}{\sigma_f^M - \sigma_s^M} \quad (2)$$

$$\text{Martensite to Austenite: } \xi = \frac{|\sigma| - \sigma_f^A}{\sigma_s^A - \sigma_f^A} \quad (3)$$

$$-\rho c V \frac{dT}{dt} = hA_S[T - T_F] - q_{gen}V \quad (4)$$

The parameter ε_L is the maximum residual strain of the material. The stress parameters from the kinetic law define the boundary lines of the transformation strips for the SMA (Figure 2), where the subscript *s* refers to the start of the phase transformation and *f* to the end of the phase transformation. Parameter ρ is the material density, *c* is the specific heat and *V* is the volume of the SMA wires. Parameter *h* is the coefficient of heat transfer by convection and A_S is the corresponding surface area of the SMA wires that can exchange heat with the environment. The term q_{gen} corresponds to the power generated per unit volume in the SMA, both by internal friction and by the latent heat from the phase transformations.

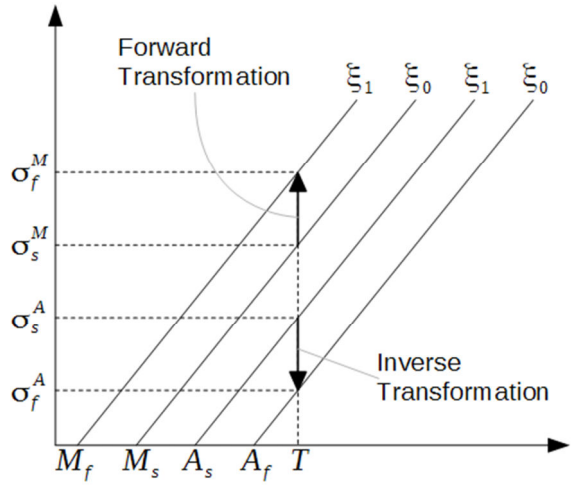

Fig. 2 - Generic SMA stress-temperature phase diagram. The four transformation temperatures (M_f, M_s, A_s and A_f) define the boundary stress values of the phase transformations for any given temperature (T) as a function of the Clausius-Clapeyron coefficient

EXPERIMENTAL TESTS

The experimental characterization process of the damper was performed using a series of cyclic traction/compression tests. At this stage no tests simulating seismic conditions were performed. The tests were conducted on a servo-hydraulic testing machine (SCHENCK HYDROPULS PSB - 500 kN) using displacement control. A load cell and a displacement transducer were used to measure the external load and the applied displacement, respectively (Figure 3). One of the SMA wires was also instrumented with a thermistor to register the average temperature changes in the material during the loading/unloading cycles The signals produced by these transducers, after being amplified and filtered by a signal conditioning system, were measured and recorded using a NI 9215 data acquisition module.

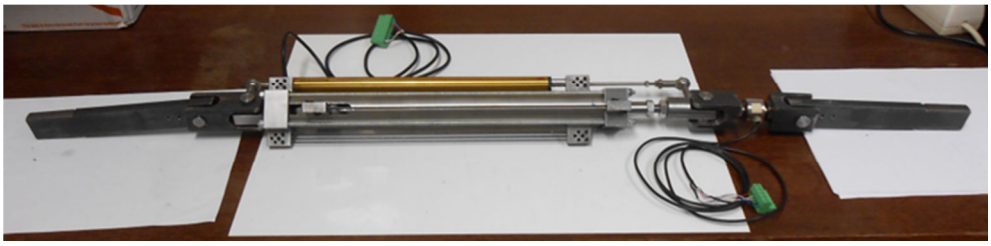

Fig. 3 - damper prototype ready to be tested

For this study, our aim was to apply loading frequencies up to 10 Hz on the damper. But after some preliminary tests, it became evident that the damper and the testing equipment couldn't handle the energy levels associated with the higher loading frequencies, mainly due to problems in the device's wire clamping solution. So using this experimentally determined input power limit, Table 1 shows the set of parameters used in each test series. Each series was performed with three repetitions and at least ten cycles per repetition, at room temperature. Table 1 also shows the average strain-rate for each test series.

Table 1 - Set of parameters used in each test series

Loading Frequency (Hz)	Test Amplitude peak to peak (mm)	Average Strain-Rate (%/s)
1	6	3.13
1	8	4.24
1	10	5.35
1	12	6.43
2	6	6.31
2	8	8.48
2	10	10.65
2	12	12.85
5	6	16.60
5	8	22.15
5	10	28.46

RESULTS

The main goal of these tests was to continue the mechanical characterization of the device, initiated in the previous testing campaign (Morais, 2017), and to determine its damping performance for higher strain-rates. To achieve this goal, the obtained results were analysed and compared to ultimately calculate the equivalent viscous damping ratio (ζ) of the device, according to equation (5) (Dolce, 2000), where E_D is the energy dissipated in each loading cycle and E_S is the maximum strain energy of the material for the same loading cycle. E_D corresponds to the area between the stress-strain curve, result of the hysteretic behaviour of the material.

$$\zeta = \frac{1}{4\pi}\frac{E_D}{E_S} \tag{5}$$

As expected, the average temperature on each wire increases continuously from the start of the test until the end or until thermal equilibrium is achieved between the heat generated by the wires and the heat extracted by the surrounding environment through convection. This

thermal equilibrium temperature value depends on the loading frequency and displacement amplitude applied to the device, and also on the environmental conditions of the test.

Figure 4 illustrates the mechanical behaviour of the device as a function of the applied displacement amplitude and loading frequency by comparing different test series. Similarly to the previous results, the graphic on the left shows that the resulting load is highly dependent on the applied displacement amplitude, while the graphic on the right illustrates that frequency changes have a lower influence on the resulting load.

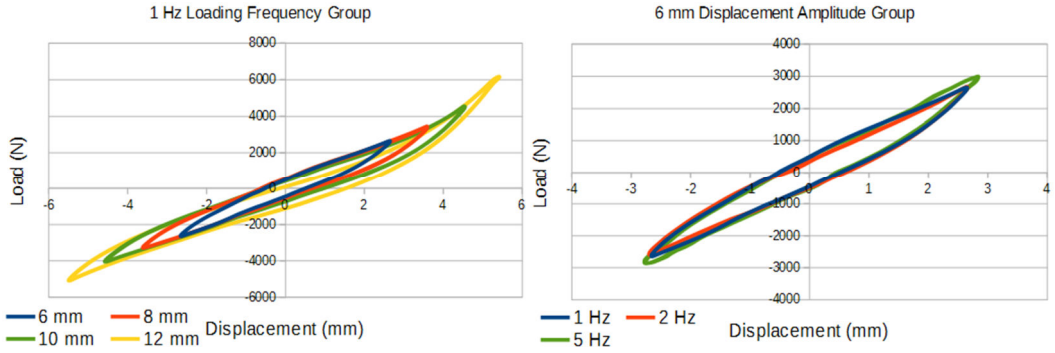

Fig. 4 - Stacked stress-strain curves of several test series to illustrate the influence of the displacement amplitude and loading frequency on the resulting load

In order to have a wider view of the damping behaviour of the device, the data collected in these tests (2018 campaign) was added to the data from the previous tests (2017 campaign). Figure 5 illustrates the device's sensitivity to strain-rate changes relative to its damping ratio. In the 2018 dataset, that represent the higher loading frequencies, the strain-rate appears to have a much lower influence on the damping ratio when compared to the 2017 dataset. In each of these tests, the thermal equilibrium temperature tended to be the same, so it is expectable that there shouldn't be any major damping ratio differences between them, as temperature changes represent one of the major parameters that can affect the damping ratio (Dolce, 2001). This is true for the specific conditions of these tests, such as room temperature and convection conditions, applied amplitude and loading frequency ranges, and specific SMA being tested.

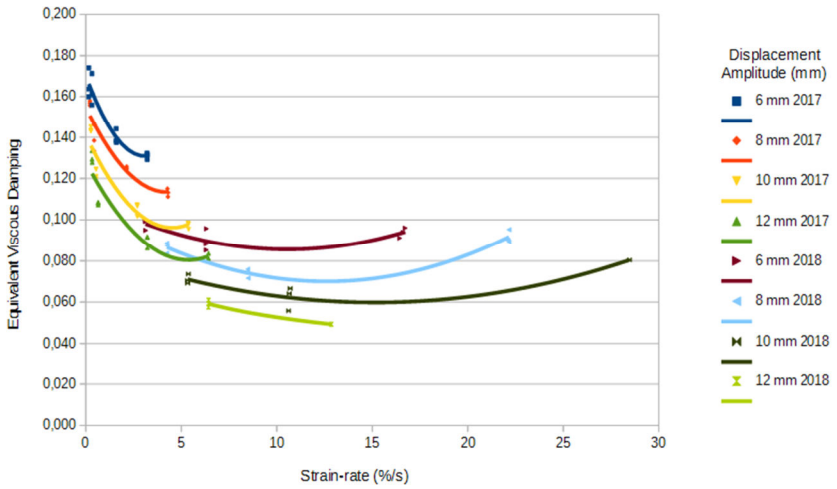

Fig. 5 - Influence of strain-rate on the device's damping ratio. This graphic includes data from 2017 and 2018 tests

Upon a closer look at the data collected from both test campaigns, there is evidence of a severe drop in the damping ratio from the 2017 tests to the 2018 tests, even for similar testing parameters. This is likely due to an ageing effect on the wires, since the device was left under pre-strain between both test campaigns, for a span of almost nine months. Figure 6 gives further evidence of this claim, by comparing two similar test sets from 2017 and 2018. In both cases, the area between the loading curve is narrower for the 2018 tests, which results in less energy dissipated per loading cycle and hence a smaller damping ratio. The damping ratio dropped from 0.13 to 0.1 for the 6 mm displacement amplitude test sets and from 0.098 to 0.07 for the 10 mm displacement amplitude test sets. This behaviour is in accordance with the information available in the literature on this subject (Isalgue, 2015).

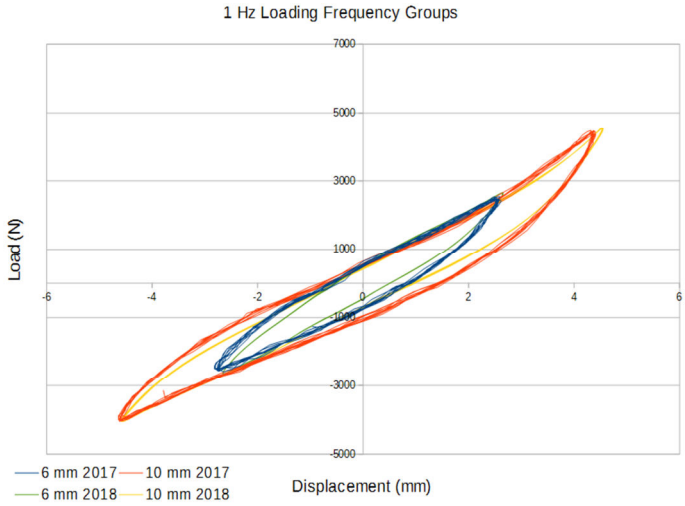

Fig. 6 - Ageing effect on the damping capability of the device

Next, using the wire temperature data acquired, the three repetitions from the several tests were compared. Here it became evident the decrease in the damping ratio due to an increase in the average wire temperature. The temperature changes during each test can be attributed to two factors: internal friction in the material due to the loading cycles and the latent heat generated by the phase transformations (Dolce, 2001). This effect is related to the Clausius-Clapeyron coefficient and its interaction with the damping capability of SMA wires. Figure 7 shows one of these comparisons, where the temperature increase is relatively small, and so the damping ratio decrease is also small, but noticeable, between the three repetitions.

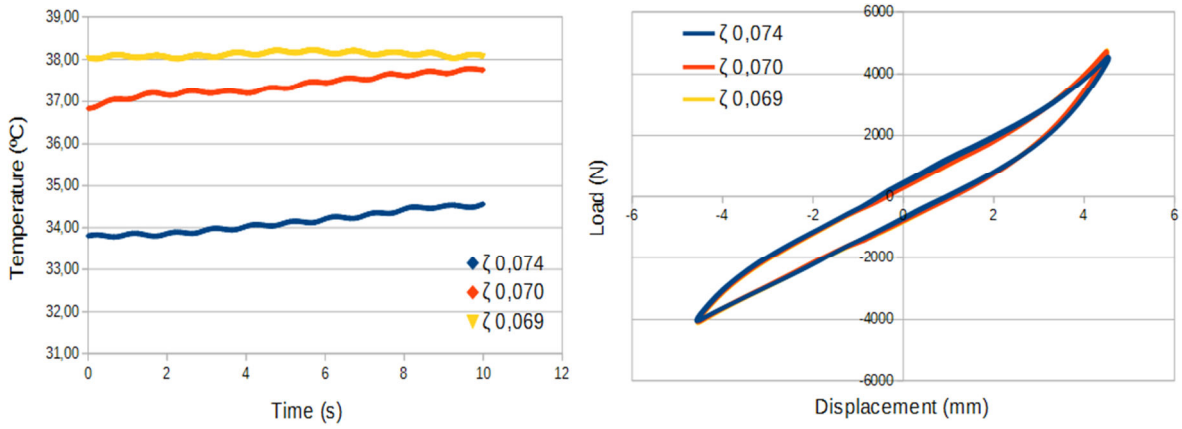

Fig. 7 - Temperature effect on the damping capability of the device, due to internally generated heat

Finally, in order to gauge the capability of our constitutive model to reproduce experimental tests, several simulations were made against the collected data. Figure 8 shows one of these simulations, using one test from the 2017 group with 6 mm of displacement amplitude and 0.05 Hz of loading frequency. While the model is not fully able to reproduce the damper behaviour, it is adequate for design purposes. It is also able to predict, by excess, the device's damping capabilities for any given situation and loading path.

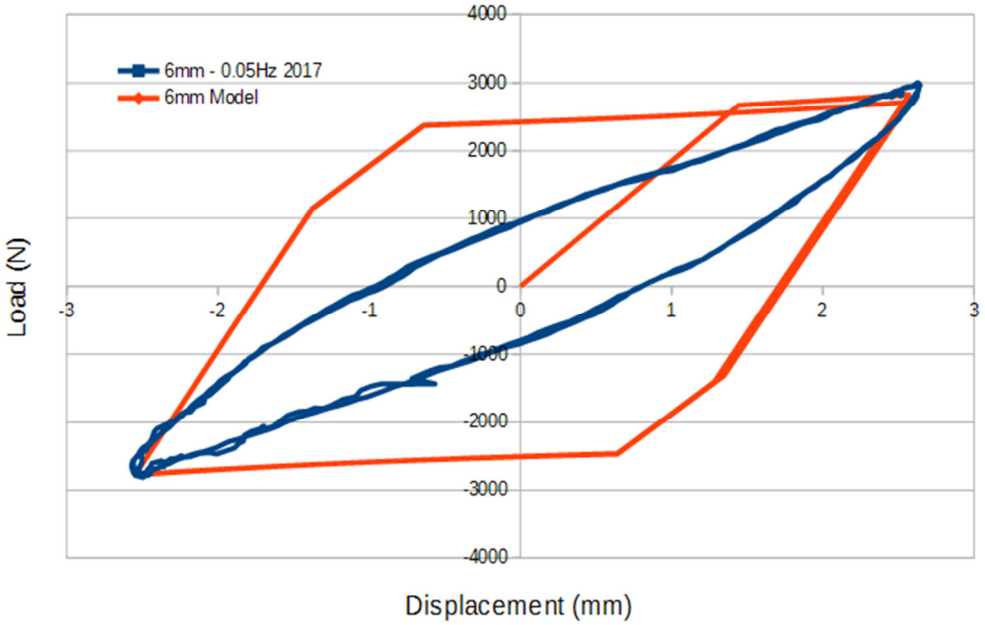

Fig. 8 - Stress-strain curves comparing experimental data (6 mm - 0.05 Hz) with the constitutive model

Figure 9 shows another of these simulations from the 2017 group, now with 12 mm of displacement amplitude and 1 Hz of loading frequency. Here the model is still unable to fully replicate the damper behaviour, but is capable of simulating higher strain-rate tests.

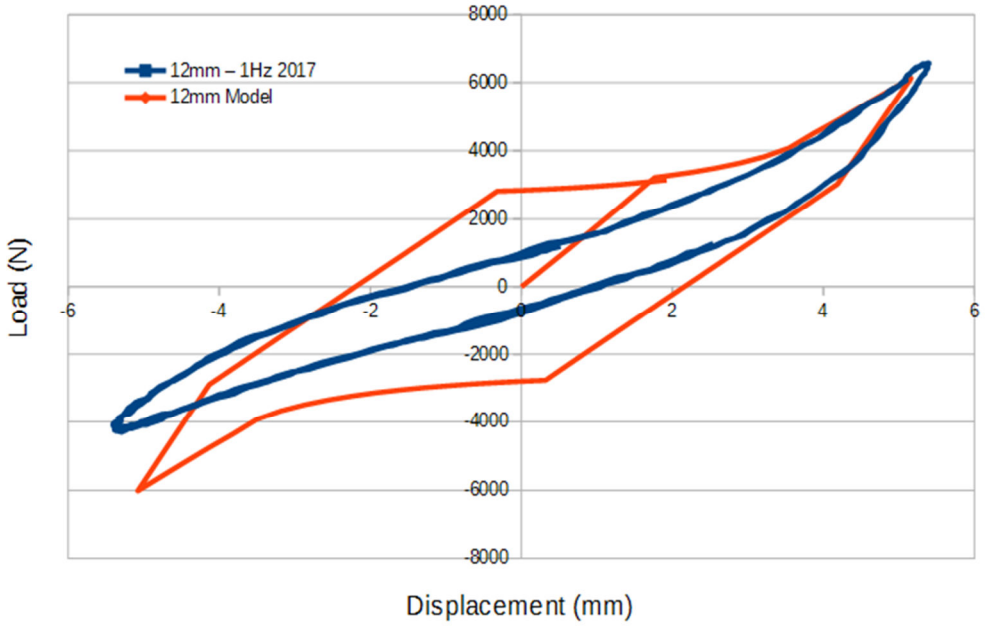

Fig. 9 - Stress-strain curves comparing experimental data (12 mm - 1 Hz) with the constitutive model

After analysing these simulations, there are two aspects where improvements could be made to improve the quality of the results. The first aspect is to experiment with other kinetic laws, like the cosine law and the exponential law described in the literature (Lobo, 2015). The second aspect is to refine the material parameters used for these simulations, since the parameters used in this study were based on the factory material parameters, supplied by the manufacturer, and so didn't took into account the changes caused by the high number of cycles effect and the ageing effect. Both the 2017 and 2018 test campaigns exhibited the high number of cycles effect, since the wires used in these tests had definitely been subjected to more than 100 cycles prior to the tests (Dolce, 2001 and Isalgue, 2015). The 2018 campaign wasn't used in these simulations because it also exhibited the ageing effect.

CONCLUSIONS AND FUTURE WORK

This paper presented the mechanical characterization process of a SMA wire based damper for high strain-rates, in the context of earthquake response mitigation. Here the damper exhibited relatively low changes on its damping ratio for these high strain-rates. This could be an interesting feature for this specific application, since in the earthquake characteristic frequency range [0.2 - 4 Hz] (Dolce, 2001), the device has a near constant response to external excitation, regarding its damping ratio.

Future work on this subject, in order to further verify this behaviour, will include the development and implementation of an improved wire clamping solution. To verify if improvements can be made to the damping capabilities of the damper for these higher strain-rates, a solution to improve the heat extraction by convection during the tests will be implemented and tested. Regarding the constitutive model, in our opinion, it is now an acceptable tool from a design perspective. Certainly improvements can be made to further refine the quality of the results. This will also be included in future work on this subject.

REFERENCES

[1] Morais J, Morais P, Santos C, Campos Costa A, Candeias P. Shape Memory Alloy Based Dampers for Earthquake Response Mitigation. 2nd International Conference on Structural Integrity, 2017.

[2] Lobo P, Almeida J, Guerreiro L. Shape memory alloys behaviour: A review. 1st International Conference on Structural Integrity, 2015.

[3] Dolce M, Cardone D, Marnetto R. Implementation and testing of passive control devices based on shape memory alloys. Earthquake Engineering and Structural Dynamics, 2000.

[4] Dolce M, Cardone D. Mechanical behaviour of shape memory alloys for seismic applications. International Journal of Mechanical Sciences, 2001.

[5] Auricchio F, Fugazza D, DesRoches R. Numerical and Experimental Evaluation of the Damping Properties of Shape-Memory Alloys. Journal of Engineering Materials and Technology, 2006.

[6] Tanaka K, Kobayashi S, Sato Y. Thermomechanics of transformation pseudoelasticity and shape memory effect in alloys. International Journal of Plasticity 2, 1986.

[7] Isalgue A, Auguet C, Torra V, Carreras G, Lovey F. Effects of strain aging in NiTi SMA wire for dampers. International Conference on Martensitic Transformations, 2015.